

Letter



⊘ Cite This: Environ. Sci. Technol. Lett. 2019, 6, 365–371

pubs.acs.org/journal/estlcu

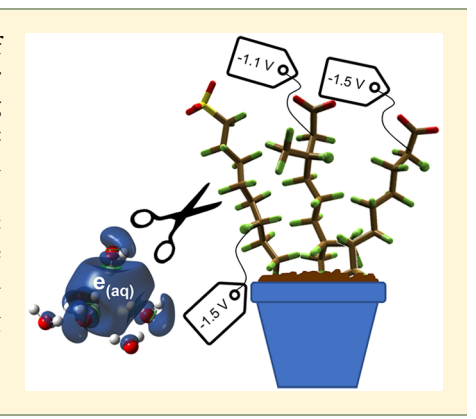
Early Events in the Reductive Dehalogenation of Linear Perfluoroalkyl Substances

Daniel J. Van Hoomissen and Shubham Vyas*

Department of Chemistry, Colorado School of Mines, 1012 14th Street, Golden, Colorado 80401, United States

Supporting Information

ABSTRACT: This work details the early events in the reductive defluorination of perfluoroalkyl substances (PFASs) and presents a straightforward methodology for predicting the reduction behavior of the perfluoroalkyl acids (PFAAs) using electronic structure calculations. Electron attachment to linear perfluorocarboxylic acids generally occurs at the α -carbon and is energetically not correlated to chain length, contrary to the case for linear perfluoroalkanesulfonates, where electrons generally insert into other positions. Perfluorooctanesulfonate and perfluorooctanoic acid, two widely studied and scrutinized PFAAs, are therefore predicted to be reduced through diverging pathways. Our protocol can predict the standard reduction potentials of PFAAs, provides a rational basis for probing reaction intermediates, establishes free energy relationships, and accounts for PFASs' inherent structural diversity beyond the linear substrates.



INTRODUCTION

Widespread biosphere contamination by perfluoroalkyl substances (PFASs) has become a worldwide dilemma¹ after decades of pervasive and largely unregulated use. The chemical recalcitrance and potential for bioaccumulation^{2,3} of PFASs has instigated a worldwide effort to detect PFAS in the environment^{4,5} and also mitigate the pathways of exposure.⁵ As the epidemiological implications of PFAS-based pollution have become recognizable outside of scientific circles, many studies continue to highlight the troubling aspects of acute and chronic toxicity.6 The growing body of evidence of the negative impacts to human physiology, coupled with their continued and worldwide use, warrants a more concerted effort to understand PFAS degradation on a molecular level. Studies describing oxidative degradation techniques and their associated mechanisms are prevalent in the literature; 8-10 however, theoretical and mechanistic studies concerning reductive techniques are scarce. The semiempirical work of Forest et al., 11 the analysis of electron attachment to gas-phase n-perfluoroalkanes (n-PFAs) by Paul et al., 12 and the recent exploration of the kinetic aspects of perfluorooctanoic acid (PFOA) reduction via zerovalent metals by Blotevogel et al. 13 are some noteworthy exceptions. Our work aims to reframe and expand our knowledge of how PFASs are reduced at the molecular level.

MATERIALS AND METHODS

All stationary points were located with three density functionals, B3LYP, $^{14-16}$ M06-2X, 17 and ω B97-XD, 18 with 6-311+G(2d,2p) basis sets using the Gaussian 09(d.01) software suite. 19 Hessian calculations were used to verify whether the structure was a minimum or maximum, and the SMD implicit solvent model²⁰ was utilized throughout to mimic an aqueous

environment. The Natural Bond Orbital (NBO 3.1,21 Gaussian09) method provided atomic spin densities and charges. All PFAAs were assumed to be in a deprotonated (anionic) form (see the list of acronyms in the Supporting Information). Standard reduction potentials (E_s°) were calculated against the standard hydrogen electrode (SHE = 4.44 V) via eq 1.

$$E_{\rm s}^{\circ} = \frac{\Delta G_{\rm (SMD)}}{nF} - \text{SHE} \tag{1}$$

■ RESULTS AND DISCUSSION

PFBS and PFPeA as Model Systems for Electron **Attachment.** First, we qualitatively explored the attachment of electrons (e⁻) to perfluorobutanesulfonate (PFBS) and perfluoropentanoic acid (PFPeA). The relaxed potential energy surface (PES) scans at the B3LYP level revealed the intermediates following e insertion (section S2 of the Supporting Information). Upon reduction, the pathways leading to the dissociation of the C-F bond were the most thermodynamically favorable (Figures S1-S16). The geometries and NBO populations of the optimized e- adducts for PFPeA and PFBS were indicative of dissociative e⁻ attachment processes resulting in weakly bound, noncovalent complexes between the fluoride and the radical anion (Figure 1).

Thermodynamically, the most favorable position for e insertion was directly dependent on whether the compound was a carboxylate or sulfonate (Table 1). Aqueous one-

Received: March 22, 2019 Revised: April 9, 2019 Accepted: April 10, 2019 Published: April 10, 2019



Environmental Science & Technology Letters

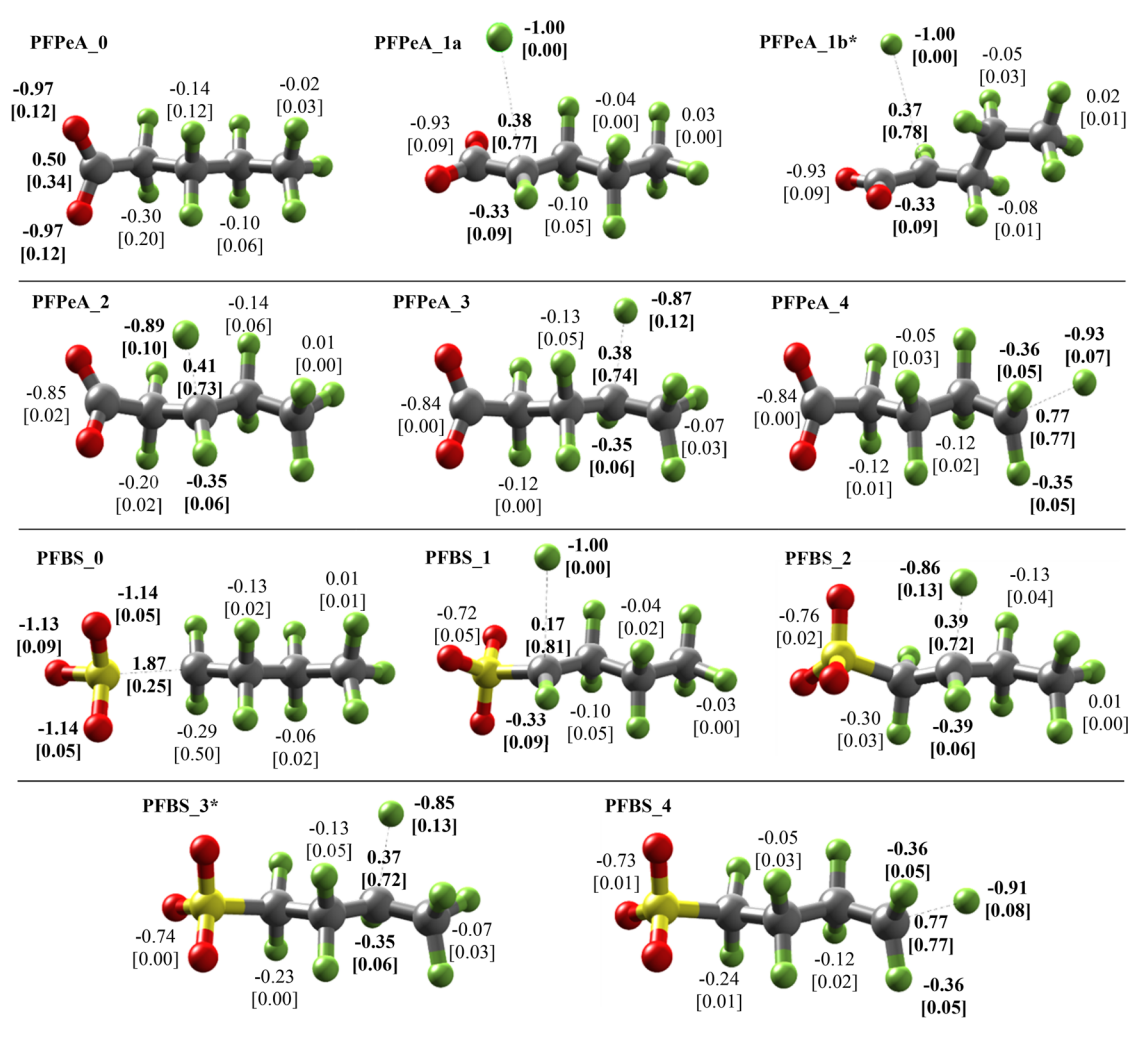


Figure 1. Intermediate radical-dianion conformations after electron attachment to PFPeA and PFBS with the position indicated by "structure_carbon number". NBO partial atomic charges and excess α-spin densities (in brackets) are given for "atom groups" except where the extra electron is present (bold values) in which all atomic centers are given. Asterisks denote the lowest-energy conformations using ZPE-corrected energies at the B3LYP(SMD)/6-311+G(2d,2p) level.

Table 1. Relative Bottom-of-the-Well ($\Delta E_{\rm rel,HF}$) and Zero-Point-Corrected Energies ($\Delta E_{\rm rel,ZPE}$), C-F Bond Lengths (angstroms) for Each Electron Attachment Location, C-F Bond Dissociation Energies of the Parent Molecule (kilojoules per mole), and One-Electron Reduction Potentials for Conformations Shown in Figure 1 (volts) (SHE = 4.44 V) at the B3LYP(SMD)/6-311+G(2d,2p) Level of Theory

	$\Delta E_{ m rel,HF}$	$\Delta E_{ m rel,ZPE}$	R_{C-F}	BDE_{C-F}	$E_{\rm s,com.}^{\circ}$	$E_{ m s, sep.}^{\circ}$
PFPeA_0	131.5	128.9	_	-	-2.99	_
PFPeA_1a	2.4	2.1	3.665	439.4	-1.50	-1.22
PFPeA_1b ^a	0	0	4.001	441.8	-1.52	-1.26
PFPeA_2	12.3	12.8	2.386	450.5	-1.74	-1.32
PFPeA_3	7.3	6.9	2.374	452.6	-1.64	-1.34
PFPeA_4	45	44.8	2.501	490.1	-2.02	-1.76
PFBS_0	44.3	42	_	_	-2.02	_
PFBS_1	8.8	9.2	3.547	454.3	-1.61	-1.32
PFBS_2	8.4	8.8	2.336	440.7	-1.72	-1.19
PFBS_3 ^a	0	0	2.309	448.8	-1.61	-1.26
PFBS_4	38.5	38.55	2.439	489.4	-2.00	-1.74

^aLowest-energy conformation.

electron reduction potentials were computed by treating the intermediates as complexed $(E_{s,com.}^{\circ})$ or dissociated/infinitely separated $(E_{s,sep.}^{\circ})$ products; $E_{s,sep.}^{\circ}$ values were less negative due to entropic effects. The aqueous reduction potentials computed generally correlated with the bond dissociation energy (BDE) of the parent monoanion's C-F bond. Attachment of an electron to PFPeA occurs near the α -carbon (C1) (to the headgroup) and results in complete dissociation of the C–F bond, while for PFBS, e^- insertion occurs at the γ carbon (C3) and forms a stable intermediate. PFPeA 1a and PFPeA 1b are the most stable because the radical is resonance-stabilized by the π -system of carboxylate. Blotevogel et al. also predicted reduction of the α -carbon for PFOA that was predicated by computing C-F BDEs at the M06-2X level. 13 The sulfonate's trigonal geometry in PFBS_1a cannot impart the same π -stabilization, which is evident by contrasting the spin/charge populations between PFPeA 1a/1b and PFBS 1a. Desulfurization (PFBS 0), proposed in the ultraviolet-sulfite-mediated reduction of PFOS, 22 was also found to be thermodynamically favorable. Structures akin to PFPeA 0 have been previously proposed as photoreduction intermediates, ^{23,24} and PFPeA 0 was the only observed case of nondissociative e- attachment. NBO analysis of PFPeA 0

Environmental Science & Technology Letters

Scheme 1. Proposed Mechanism for Two-Electron Reduction for PFPeA 0 in (1) Organic Nonprotic Solvents and (2a) Explicit Aqueous Conditions for PFPeA 1a and (2b) the Implicit Stepwise Pathway for PFPeA 1ba

"After the first reduction and fluoride release (red atom), the carbo-radical can undergo a second reduction, releasing fluoride (blue atom) in the organic solvent or under aqueous conditions can undergo reaction with water (green atoms) to form H-incorporated compounds.

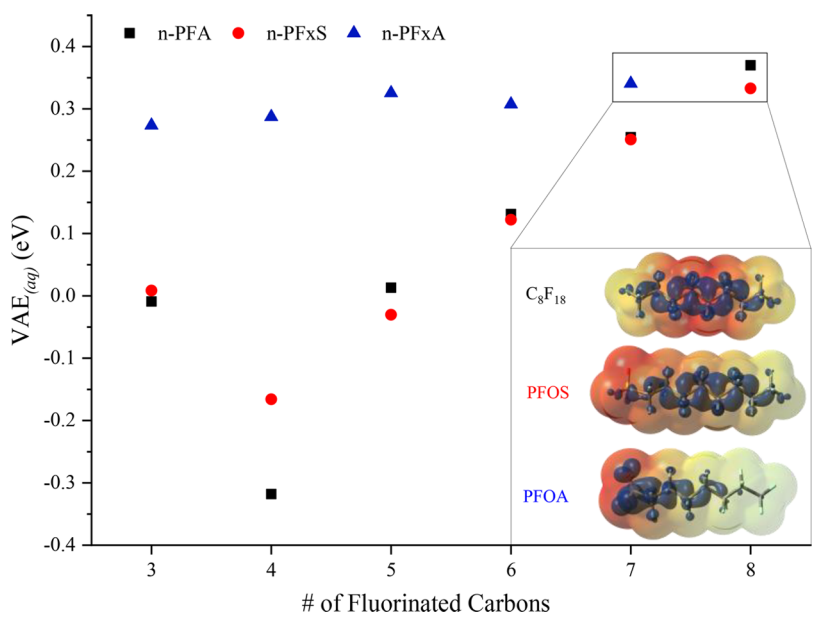


Figure 2. Aqueous vertical attachment energies of n-PFAs, n-PFxSs, and n-PFxAs at the ωB97-XD(SMD)/6-311+G(2d,2p) level. The inset shows the electrostatic potential overlaid on the total electron density (isoval = 0.001) and the α -spin-density isosurfaces (isoval = 0.001) for PFOA^{2-•}, PFOS^{2-•} and $C_8F_{18}^{-•}$.

illustrates that the additional e is mostly centered on the carboxylate, indicating the influence of the $\pi_{C=O}^*$ orbitals on reactivity. A barrier-less transition state structure that connects PFPeA 0 and PFPeA 1b was identified and represents one of many possible mechanisms for attachment of e to PFxAs leading to F⁻ discharge (Scheme 1 and Figure S18).

Following the first reduction and F⁻ release, the geometry of the anion radical and the presence of a protic solvent have sweeping implications for its subsequent reactivity (Scheme 1). Contrary to the mechanism suggested by Qu et al., we found abstractions of radical H atoms from a water molecule kinetically and thermodynamically unfavorable.²⁵ However, perfluoro-dianion species created by a second reduction can abstract a proton from water in a kinetically favorable and nearthermoneutral process (Tables S1-S4). Double bond formation, suggested in VB12-mediated reductive defluorination of branched PFxS, 26 was also observed following the second reduction of PFPeA 1a, except when explicit water molecules formed hydrogen bonds with the carbanion. Full

consideration of the solvent's role in PFAS reduction was beyond the scope of this work; nonetheless, these results corroborate previously proposed mechanisms, ^{24,27} including those hypothesizing that hydrogen is incorporated into the C-C backbone. 23,26,28,29

Benchmarking Computational Methods: n-PFAs and Instantaneous Electron Attachment. Concurrently, we assessed instantaneous attachment of electrons to various (C₃-C₈) n-PFAs, n-PFxSs, and n-PFxAs (C₃ excluded) by computing vertical attachment energies (VAEs). VAEs, while typically computed in the literature for gas-phase species, were computed with the SMD continuum solvation model for a direct chemical comparison. In these cases, the (aq) descriptor will symbolize electron affinities computed with the SMD model. Previously, the energies and the spatial extent of the unoccupied molecular orbitals in the parent compounds provided early mechanistic conclusions concerning PFAS reduction²² and were used to develop linear free energy relationships (LFERs).¹¹ We found the distribution and

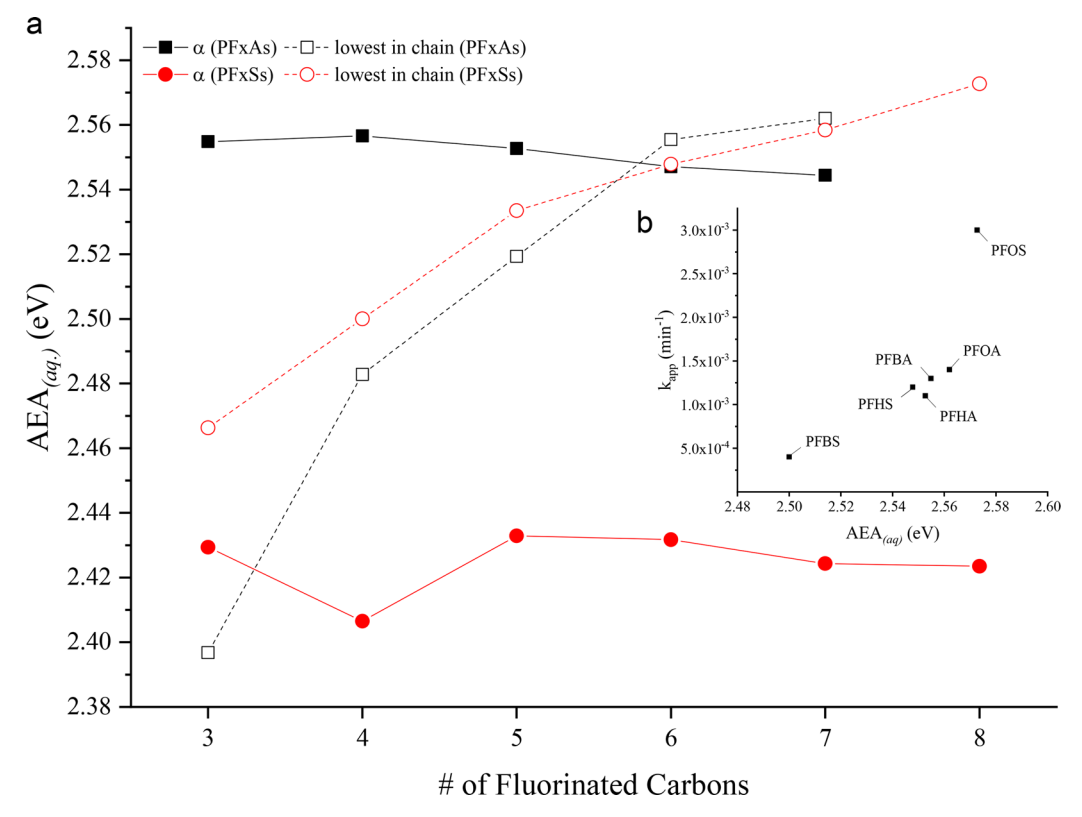


Figure 3. (a) Comparison of AEA_(aq)s of position α and the (next) most favorable attachment positions for PFxAs (black) and PFxSs (red). (b) Relationship between experimental $k_{\rm app}$ values²⁺ (ultraviolet—iodide) and theoretical AEAs for PFxAs and PFxSs. and All values are ZPE-corrected electronic energies obtained at the ω B97-XD(SMD)/6-311+G(2d,2p) level.

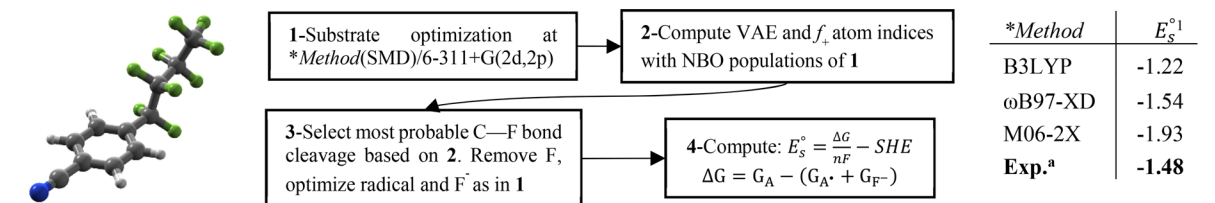
energetics of the first occupied and the next three unoccupied molecular orbitals to be method-dependent for all three subclasses of PFASs; therefore, we felt it necessary to move beyond this qualitative marker (section S8).

Spin-density isosurfaces, which provide the spatial distribution of the additional e⁻, showed that inner-chain σ_{C-F}^{ϵ} orbitals are the most susceptible to reduction in n-PFAs (Table S5 and Figure S19). From an energetic standpoint, the VAE_(aq)s in PFxAs did not significantly change with an increase in chain length in contrast to the PFxSs and n-PFAs (Figure 2). The M06-2X-based results (Figure S20) complemented these trends, but the B3LYP-based results showed that all three subclasses have roughly similar VAE_(aq) behavior (Figure S21). The spin-density isosurfaces and the electrostatic potential maps revealed that PFOS and perfluorooctane stabilize the e⁻ along the perfluoroalkyl chain, juxtaposed with PFOA, in which the e⁻ appeared to be delocalized across both π_{C-F}^* orbitals.

Subsequently, we computed the relaxed structures for the n-PFAs (C_3-C_8) , n-PFxAs (C_4-C_8) , and n-PFxSs (C_3-C_8) and repeated previous gas-phase computations for the n-PFAs; both illustrated similar electron attachment behavior (sections S5 and S6, Figure S19, and Tables S6–S8). However, the DFT functional chosen had notable consequences for the energies and geometries (Figure S22). The electron adducts for the PFxSs and PFxAs were computed using two methods: (1) by following the path of the instantaneous attachment from the parent geometry to a minimum and (2) by systematically extending each unique C–F bond of each substrate. Using the latter method, attachment of e⁻ to the α -carbon position was generally the most favorable for the PFxAs; however, in larger PFxAs, attack in the perfluoroalkyl chain became more

thermodynamically favorable (Tables S9-S16). We observed this behavior for only the PFxAs (Figure 3) and again noticed significant entropic effects when the PFxAs α -adducts were treated as infinitely separated (Tables S17 and S18). Entropic effects on the trends in Figure 3 were notable, although the conclusions remained the same (Figures S23 and S24). The results obtained through the first method were dependent on the functional form (Figures S25-S27) and are likely related to the small differences we observed in the distribution of the unoccupied orbitals in the parent compounds (section S8). For example, for PFOA, ωB97-XD predicted nondissociative eattachment at the α -carbon, B3LYP predicted nondissociative e- attachment across the chain, and M06-2X predicted C-F dissociation at position C5. Although, the first method provided meaningful insights into the structural motifs possible after e attachment, the second methodology, whose results are presented in Figure 3, allowed for a more consistent evaluation of attachment of e⁻ to PFAAs. Despite theory's lack of definitive predictions, the experimental conclusions regarding the chain length of a PFxA and their rate of reduction also remain unclear; e.g., no dependence was noted in ultraviolet-iodide-based photoreduction²⁴ but was in ultraviolet-Fe(CN)₆-based laser flash photolysis work.³⁰ Regardless, Figure 3b and Figures S23b and S24b illustrate that a relationship exists between the observed rate constants in the former work and AEA(aq)s of PFxSs and PFxAs with the same chain length.²⁴ The larger deviation observed for PFOS could be attributed to the larger errors associated with measuring [PFOS] and/or the fact that PFOS is also composed of more easily reducible branched isomers that contributed to larger observed rate constants.²⁴

Scheme 2. Computing E_s° Values of PFASs^a



"Example shown for 4-(perfluorobutyl)-benzonitrile (left). Computed standard reduction potential (Es) vs SHE (right) shown for *Method(SMD=DMF)/6-311+G(2d,2p). 1 SHE = 4.44 V. 2 Combellas et al. 27 f_{+} is the Fukui-plus function.

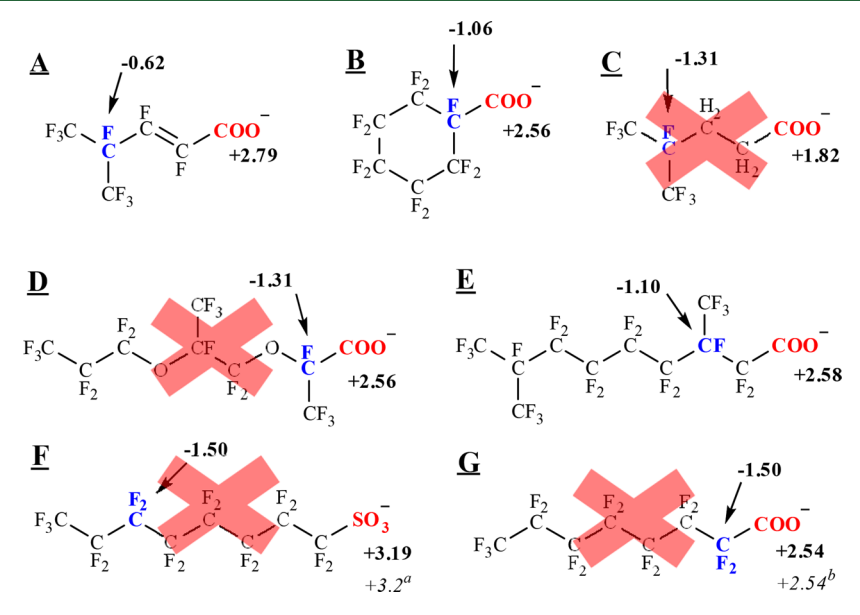


Figure 4. Calculated E^o values (in volts) for various PFAS substrates. The blue atoms represent the proposed site of chemical reduction, while red represents chemical oxidation via Scheme 2. Literature values (italics) are from a Carter and Farrell 3 and Guan et al. 3 Structures with a red X were resistant to Co(I)-corrin defluorination as described by Liu et al.3

Predicting the Redox Behavior of n-PFAAs and Beyond. The preceding analysis allowed for a systematic approach to elucidating attachment of e to linear PFAS; however, these parameters are not easily obtained and rationalized through routine experimentation. To provide more meaningful predictions, we devised a cogent, stepwise method for predicting the E_s° of PFASs (Scheme 2). Using 4-(perfluorobutyl)-benzonitrile as an example substrate, the ω B97-XD(SMD)/6-311+G(2d,2p) method predicted an E_s° within 0.1 V of the experimental result.²⁷ We found reasonably good agreement between theory and experiment was reached when F and the radical intermediate were treated as infinitely separated species. Therefore, all preceding computations were subject to this constraint. Although this was not an original focus of this work, Scheme 2 can also predict the oxidation potential of various PFAAs using $E_{s,com.}^{\circ}$ instead of $E_{s,sep.}^{\circ}$ in an analogous technique presented recently by Baggioli et al. 31 For example, the reduction of PFOA $^{\bullet}$ ($E_s^{\circ} = 2.54$ V, comp. and exp. 32) and PFOS• ($E_s^{\circ} = 3.19 \text{ V comp.}, E_s^{\circ} = 3.20 \text{ exp.}^{33}$) can be accurately reproduced. Baggioli et al. suggested B3LYP-(PCM) or TPSSh(SMD) is a more suitable alternative, and although they predict lower E_s° values for PFOA $^{\bullet}$ (~2.2 V), it is in qualitative agreement with cyclic voltammetry experiments with PFOA in acetonitrile. 31,34 Accordingly, Scheme 2 in conjunction with the ω B97-XD-based method was utilized to compute both the reduction and oxidation potentials for a

diverse set of PFAA substrates, including multifunctional and branched species (Figure 4).

Figure 4 shows PFAA oxidation is dependent on the headgroup and independent of the perfluoroalkyl chain length, with e loss typically occurring at or near the acidic moiety. Conversely, reduction is far more structure-dependent; electrons preferentially target the lowest-lying σ_{C-F}^* orbitals, typically tertiary carbon centers, and from resonance-stabilized positions, if present.¹² The substrates shown in Figure 4 reflect our recent work on cobalt-mediated reductive defluorination³⁵ and show that the presence of tertiary C-F bonds does not guarantee outer-sphere reactivity, with C and D being notable exceptions. As the E_s° values of Co(II)/Co(I) in corrin derivatives are typically measured between -0.96 and -1.36 V (vs NHE), ^{36,37} our method illustrates the substrates amenable to Co(I) reduction. Although E_s° appears to be estimated correctly on a substrate level, outer-sphere e transfers are considered less favorable compared to inner-sphere nucleophilic attack in Co-corrin-mediated reduction of chlorinated organics. 38,39 The kinetic factors of electron transfer and a complete description of the possible inner-sphere mechanisms with various reducing agents cannot be ignored in future

The reductive defluorination of PFAAs is strongly dependent on the polar headgroup and the perfluoroalkyl chain length, but structural characteristics such as branching also play important roles in the reduction mechanism. Our computational protocol suitably predicts the reactivity of PFAAs with electrons, begins to unravel their redox behavior, and will hopefully help to identify intermediates of reductive degradation. Despite the complexity of attachment of electrons to linear PFASs, reactivity is mostly dictated by σ_{C-E}^* orbitals and often results in C-F bond scission.

ASSOCIATED CONTENT

S Supporting Information

The Supporting Information is available free of charge on the ACS Publications website at DOI: 10.1021/acs.estlett.9b00116.

Geometries and bottom-of-the-well HF energies for the parent structures and their electron adducts to all positions for linear C₈F₁₈, PFOA, and PFOS (PDF) HOMO, LUMO, LUMO+1, and LUMO+2 orbital distributions (and their energies) for the parent molecules at each level of theory in the form of image files (ZIP)

■ AUTHOR INFORMATION

Corresponding Author

*E-mail: svyas@mines.edu. Telephone: 303-273-3632.

ORCID ®

Shubham Vyas: 0000-0002-5849-8919

The authors declare no competing financial interest.

ACKNOWLEDGMENTS

This work was funded by the National Science Foundation (CHE-1710079 and CHE-1807739). The authors thank John McGroarty (undergraduate researcher) for assistance and acknowledge the computational resources allocated by the high-performance computing facility at the Colorado School of Mines.

REFERENCES

- (1) Jian, J.; Guo, Y.; Zeng, L.; Liang-ying, L.; Lu, X.; Wang, F.; Zeng, E. Y. Global Distribution of Perfluorochemicals (PFCs) in Potential Human Exposure Source - A Review. Environ. Int. 2017, 108, 51-62.
- (2) Lau, C.; Anitole, K.; Hodes, C.; Lai, D.; Pfahles-Hutchens, A.; Seed, J. Perfluoroalkyl Acids: A Review of Monitoring and Toxicological Findings. Toxicol. Sci. 2007, 99, 366-394.
- (3) Parsons, J. R.; Sáez, M.; Dolfing, J.; de Voogt, P. Biodegradation of Perfluorinated Compounds; Springer: New York, 2008; Vol. 196.
- (4) Farre, M.; Kantiani, L.; Petrovic, M.; Perez, S.; Barcelo, D. Achievements and Future Trends in the Analysis of Emerging Organic Contaminants in Environmental Samples by Mass Spectrometry and Bioanalytical Techniques. J. Chromatogr. A 2012, 1259, 86-99.
- (5) Houde, M.; De Silva, A. O.; Muir, D. C. G.; Letcher, R. J. Monitoring of Perfluorinated Compounds in Aquatic Biota: An Updated Review. Environ. Sci. Technol. 2011, 45, 7962-7973.
- (6) Chang, E. T.; Adami, H.; Boffetta, P.; Wedner, H. J.; Mandel, J. S. A Critical Review of Perfluorooctanoate and Perfluorooctanesulfonate Exposure and Immunological Health Conditions in Humans. Crit. Rev. Toxicol. 2016, 46, 279-331.
- (7) Houtz, E. F.; Sutton, R.; Park, J. S.; Sedlak, M. Poly- and Perfluoroalkyl Substances in Wastewater: Significance of Unknown Precursors, Manufacturing Shifts, and Likely AFFF Impacts. Water Res. 2016, 95, 142-149.
- (8) Trojanowicz, M.; Bojanowska-Czajka, A.; Bartosiewicz, I.; Kulisa, K. Advanced Oxidation/Reduction Processes Treatment for Aqueous Perfluorooctanoate (PFOA) and Perfluorooctanesulfonate (PFOS) -A Review of Recent Advances. Chem. Eng. J. 2018, 336, 170-199.

- (9) Vecitis, C. D.; Park, H.; Cheng, J.; Mader, B. T.; Hoffmann, M. R. Treatment Technologies for Aqueous Perfluorooctane Sulfonate (PFOS) and Perfluorooctanoate (PFOA). Front. Environ. Sci. Eng. China 2009, 3, 129-151.
- (10) Kucharzyk, K. H.; Darlington, R.; Benotti, M.; Deeb, R.; Hawley, E. Novel Treatment Technologies for PFAS Compounds: A Critical Review. J. Environ. Manage. 2017, 204, 757-764.
- (11) Rayne, S.; Forest, K.; Friesen, K. J. Linear Free Energy Relationship Based Estimates for the Congener Specific Relative Reductive Defluorination Rates of Perfluorinated Alkyl Compounds. J. Environ. Sci. Health, Part A: Toxic/Hazard. Subst. Environ. Eng. 2009, 44, 866-879.
- (12) Paul, A.; Wannere, C. S.; Schaefer, H. F. Do Linear-Chain Perfluoroalkanes Bind an Electron? J. Phys. Chem. A 2004, 108, 9428-9434.
- (13) Blotevogel, J.; Giraud, R. J.; Borch, T. Reductive Defluorination of Perfluorooctanoic Acid by Zero-Valent Iron and Zinc: A DFT-Based Kinetic Model. Chem. Eng. J. 2018, 335, 248-254.
- (14) Becke, A. D. Density-Functional Thermochemistry. III. The Role of Exact Exchange. J. Chem. Phys. 1993, 98, 5648-5652.
- (15) Miehlich, B.; Savin, A.; Stoll, H.; Preuss, H. Results Obtained with the Correlation Energy Density Functionals of Becke and Lee, Yang and Parr. Chem. Phys. Lett. 1989, 157, 200-206.
- (16) Lee, C.; Yang, W.; Parr, R. G. Development of the Colle-Salvetti Correlation-Energy Formula into a Functional of the Electron Density. Phys. Rev. B: Condens. Matter Mater. Phys. 1988, 37, 785-
- (17) Zhao, Y.; Truhlar, D. G. A New Local Density Functional for Main-Group Thermochemistry, Transition Metal Bonding, Thermochemical Kinetics, and Noncovalent Interactions. J. Chem. Phys. 2006, 125, 194101.
- (18) Chai, J. Da; Head-Gordon, M. Long-Range Corrected Hybrid Density Functionals with Damped Atom-Atom Dispersion Corrections. Phys. Chem. Chem. Phys. 2008, 10, 6615-6620.
- (19) Frisch, M. J.; Trucks, G. W.; Schlegel, H. B.; Scuseria, G. E.; Robb, M. A.; Cheeseman, J. R.; Scalmani, G.; Barone, V.; Petersson, G. A.; Nakatsuji, H.; Li, X.; Caricato, M.; Marenich, A.; Bloino, J.; Janesko, B. G.; Gomperts, R.; Mennucci, B.; Hratchian, H. P.; Ortiz, J. V.; Izmaylov, A. F.; Sonnenberg, J. L.; Williams-Young, D.; Ding, F.; Lipparini, F.; Egidi, F.; Goings, J.; Peng, B.; Petrone, A.; Henderson, T.; Ranasinghe, D.; Zakrzewski, V. G.; Gao, J.; Rega, N.; Zheng, G.; Liang, W.; Hada, M.; Ehara, M.; Toyota, K.; Fukuda, R.; Hasegawa, J.; Ishida, M.; Nakajima, T.; Honda, Y.; Kitao, O.; Nakai, H.; Vreven, T.; Throssell, K.; Montgomery, J. A., Jr.; Peralta, J. E.; Ogliaro, F.; Bearpark, M.; Heyd, J. J.; Brothers, E.; Kudin, K. N.; Staroverov, V. N.; Keith, T.; Kobayashi, R.; Normand, J.; Raghavachari, K.; Rendell, A.; Burant, J. C.; Iyengar, S. S.; Tomasi, J.; Cossi, M.; Millam, J. M.; Klene, M.; Adamo, C.; Cammi, R.; Ochterski, J. W.; Martin, R. L.; Morokuma, K.; Farkas, O.; Foresman, J. B.; Fox, D. J. Gaussian 09, revision D.01; Gaussian, Inc.: Wallingford, CT, 2016.
- (20) Marenich, A. V.; Cramer, C. J.; Truhlar, D. G. Universal Solvation Model Based on Solute Electron Density and on a Continuum Model of the Solvent Defined by the Bulk Dielectric Constant and Atomic Surface Tensions. J. Phys. Chem. B 2009, 113, 6378-6396.
- (21) Glendening, E. D.; Reed, A. E.; Carpenter, J. E.; Weinhold, F. NBO, version 3.1; 2009; pp 2-3.
- (22) Gu, Y.; Dong, W.; Luo, C.; Liu, T. Efficient Reductive Decomposition of Perfluorooctanesulfonate in a High Photon Flux UV/Sulfite System. Environ. Sci. Technol. 2016, 50, 10554-10561.
- (23) Wang, S.; Yang, Q.; Chen, F.; Sun, J.; Luo, K.; Yao, F.; Wang, X.; Wang, D.; Li, X.; Zeng, G. Photocatalytic Degradation of Perfluorooctanoic Acid and Perfluorooctane Sulfonate in Water: A Critical Review. Chem. Eng. J. 2017, 328, 927-942.
- (24) Park, H.; Vecitis, C. D.; Cheng, J.; Choi, W.; Mader, B. T.; Hoffmann, M. R. Reductive Defluorination of Aqueous Perfluorinated Alkyl Surfactants: Effects of Ionic Headgroup and Chain Length. J. Phys. Chem. A 2009, 113, 690-696.

- (25) Qu, Y.; Zhang, C.; Li, F.; Chen, J.; Zhou, Q. Photo-Reductive Defluorination of Perfluorooctanoic Acid in Water. *Water Res.* **2010**, 44, 2939–2947.
- (26) Park, S.; De Perre, C.; Lee, L. S. Alternate Reductants with VB12 to Transform C8 and C6 Perfluoroalkyl Sulfonates: Limitations and Insights into Isomer-Specific Transformation Rates, Products and Pathways. *Environ. Sci. Technol.* **2017**, *51*, 13869–13877.
- (27) Combellas, C.; Kanoufi, F.; Thiébault, A. Reduction of Polyfluorinated Compounds. *J. Phys. Chem. B* **2003**, *107*, 10894–10905.
- (28) Ochoa-Herrera, V.; Sierra-Alvarez, R.; Somogyi, A.; Jacobsen, N. E.; Wysocki, V. H.; Field, J. A. Reductive Defluorination of Perfluorooctane Sulfonate. *Environ. Sci. Technol.* **2008**, 42, 3260—3264.
- (29) Song, Z.; Tang, H.; Wang, N.; Zhu, L. Reductive Defluorination of Perfluorooctanoic Acid by Hydrated Electrons in a Sulfite-Mediated UV Photochemical System. *J. Hazard. Mater.* **2013**, 262, 332–338.
- (30) Huang, L.; Dong, W.; Hou, H. Investigation of the Reactivity of Hydrated Electron toward Perfluorinated Carboxylates by Laser Flash Photolysis. *Chem. Phys. Lett.* **2007**, *436*, 124–128.
- (31) Baggioli, A.; Sansotera, M.; Navarrini, W. Thermodynamics of Aqueous Perfluorooctanoic Acid (PFOA) and 4,8-Dioxa-3H-Perfluorononanoic Acid (DONA) from DFT Calculations: Insights into Degradation Initiation. *Chemosphere* **2018**, *193*, 1063–1070.
- (32) Guan, B.; Zhi, J.; Zhang, X.; Murakami, T.; Fujishima, A. Electrochemical Route for Fluorinated Modification of Boron-Doped Diamond Surface with Perfluorooctanoic Acid. *Electrochem. Commun.* **2007**, *9*, 2817–2821.
- (33) Carter, K. E.; Farrell, J. Oxidative Destruction of Perfluor-ooctane Sulfonate Using Boron-Doped Diamond Film Electrodes. *Environ. Sci. Technol.* **2008**, 42, 6111–6115.
- (34) Park, H.; Vecitis, C. D.; Cheng, J.; Dalleska, N. F.; Mader, B. T.; Hoffmann, M. R. Reductive Degradation of Perfluoroalkyl Compounds with Aquated Electrons Generated from Iodide Photolysis at 254 Nm. *Photochem. Photobiol. Sci.* **2011**, *10*, 1945–1953.
- (35) Liu, J.; Van Hoomissen, D. J.; Liu, T.; Maizel, A.; Huo, X.; Fernández, S. R.; Ren, C.; Xiao, X.; Fang, Y.; Schaefer, C. E.; et al. Reductive Defluorination of Branched Per- and Polyfluoroalkyl Substances with Cobalt Complex Catalysts. *Environ. Sci. Technol. Lett.* 2018, 5, 289–294.
- (36) Lexa, D.; Saveant, J. M. The Electrochemistry of Vitamin B12. Acc. Chem. Res. 1983, 16, 235–243.
- (37) Johnston, R. C.; Zhou, J.; Smith, J. C.; Parks, J. M. Toward Quantitatively Accurate Calculation of the Redox-Associated Acid-Base and Ligand Binding Equilibria of Aquacobalamin. *J. Phys. Chem. B* **2016**, *120*, 7307–7318.
- (38) Heckel, B.; Cretnik, S.; Kliegman, S.; Shouakar-Stash, O.; McNeill, K.; Elsner, M. Reductive Outer-Sphere Single Electron Transfer Is an Exception Rather than the Rule in Natural and Engineered Chlorinated Ethene Dehalogenation. *Environ. Sci. Technol.* **2017**, *51*, 9663–9673.
- (39) Ji, L.; Wang, C.; Ji, S.; Kepp, K. P.; Paneth, P. Mechanism of Cobalamin-Mediated Reductive Dehalogenation of Chloroethylenes. *ACS Catal.* **2017**, *7*, 5294–5307.